Journal of Power Sources 222 (2013) 218–224

Contents lists available at SciVerse ScienceDirect

Journal of Power Sources

journal homepage: www.elsevier.com/locate/jpowsour

An ion exchange route to produce WO_3 nanobars as Pt electrocatalyst promoter for oxygen reduction reaction

Zaoxue Yan, Wei Wei, Jimin Xie*, Suci Meng, Xiaomeng Lü, Jianjun Zhu

School of Chemistry and Chemical Engineering, Jiangsu University, Zhenjiang 212013, China

HIGHLIGHTS

- WO_3 nanobars (3 nm × 10 nm) is synthesized through ion exchange route.
- The long-chain of the ion exchange resin results in the bar shape of WO_3.
- The shape of WO_3 varies with the concentrations of WO_3 precursor.
- WO_3 nanobars give highly promotion effect on Pt/C electrocatalyst.
- Pt/WO_3 has higher electrochemical stability than Pt/C.

ARTICLE INFO

Article history:
Received 21 June 2012
Received in revised form
18 August 2012
Accepted 22 August 2012
Available online 1 September 2012

Keywords:
Tungsten oxide
Fuel cell
Oxygen reduction reaction
Platinum electrocatalyst
Synergistic effect
Electrochemical stability

ABSTRACT

WO_3 nanobars with the length of 10–50 nm and the width of 3–6 nm on carbon (C-WO_3) are synthesized through an ionic exchange route to locally anchor the metatungstate ions ($W_7O_{24}^{6-}$). The structures, morphologies and catalytic performance of the as-synthesized nanomaterials are characterized by various physical and electrochemical methods. The results indicate that Pt nanoparticles supporting on C-WO_3 (Pt/C-WO_3) are highly active and stable as cathode electrocatalyst for fuel cells. On one hand, a mass activity of 174.6 mA mg^{-1}_{Pt} at 0.9 V is obtained for oxygen reduction reaction (ORR), which is much higher than that on commercial Pt/C electrocatalyst (98.6 mA mg^{-1}_{Pt}). On the other hand, Pt/C-WO_3 electrocatalyst shows excellent electrochemical stability than Pt/C. The origin of these improvements in the catalytic activity can be attributed to the synergistic or promotion effect of WO_3 on Pt. The improvement in the electrochemical stability is due to and also explains the stronger interaction force between Pt and WO_3 than that between Pt and C. The present method is simple and effective, which can be readily scale up for the production of other nanomaterials as well as WO_3.

1. Introduction

Low temperature fuel cell technology has been considered as one of the important ways to decrease the energy crisis of the world for its high-energy conversion efficiency, so it has great and potential economic value [1–5]. The electrocatalyst is the critical part of the low temperature fuel cells. Owing to the sophisticated synthesis technologies, relatively good electrochemical activity and stability, noble metals such as Pt and Pd have been remaining the main active ingredients of the electrocatalysts [2,6–9]. However, the high cost of the noble metals restricted the popular application of the low temperature fuel cells, especially for the cathode side which need more amount of noble metals to promote the kinetics of the oxygen reduction reaction (ORR) [10–12]. On the other hand, the carbon support corrosion remains the major challenges for high potential on fuel cell ORR electrocatalysts [13]. Therefore, many efforts such as structure design, alloy synthesis and crystal parameter alteration on the noble metal have been made to obtain improved electrocatalytic activity, stability and use ratio [2,8,14–16]. On the above basis, graphitization or composite synthesis on the carbon support to achieve more stable catalyst structure and performance was also exposited [3,7,17,18].

Metal oxides have aroused much attention and been studied in various fields including light-emitting diodes [19,20], coating materials [21], photocatalysis [22–24], flame retardants [25], chemi-sensors [26,27], solar cells [28,29] and catalytic reaction [30,31]. Due to their promotion effect on noble metal electrocatalyst, metal oxides were also investigated with interesting as electrocatalyst promoter for fuel cells, which have been approved to be able to improve the overall catalytic activity to a large degree

* Corresponding author. Tel: +86 11 88791708; fax: +86 11 88791800.
E-mail addresses: earlylearn@163.com, Xiejm391@sohu.com (J. Xie).

0378-7753/$ – see front matter
http://dx.doi.org/10.1016/j.jpowsour.2012.08.070

[32–34]. Specially, it has been reported that tungsten oxides have excellent CO tolerance and higher catalytic activity when being loaded with Pt nanoparticles as electrocatalysts [35–41]. According to Savadogo's report, the electrocatalytic activity of Pt supporting on WO_3 for ORR in acidic media was twice as high as that of Pt supporting on carbon [42].

There have been many methods for the synthesis of tungsten oxides with various shapes including nanowires [39,40], nanofilms [43], nanoclusters [44], microfibers [45], etc. It is believed that the big particles of promoter catalyst are difficult to exert the promotion effect on noble metal electrocatalysts. The reason is that they have too heavy density and low specific surface area to perform the promotion effect efficiently and disperse the noble metal particles uniformly [46,47]. So it is of great significance to develop nanosized metal oxides with a controllable size down to 10 nm or less.

Here, we synthesized WO_3 nanobars with the length of 10–50 nm and the width of 3–6 nm that were uniformly dispersed on carbonized resin (C-WO_3) through ionic exchange route [3,7,18]. The WO_3 nanobars synthesized here were used as Pt electrocatalyst promoter for ORR in acidic media and showed excellent electrochemical stability as well as remarkable catalytic promotion effect.

2. Experimental

Typically, the D201 × 1 cinnamic strong alkali anion exchange resin (10 g, Hebi Power Resin Factory, China) was impregnated in 100 ml of AMT (ammonium metatungstate, $(NH_4)_6W_7O_{24}\cdot 6H_2O$, A.R., Tianjin Jinke Fine Chemicals Co., China) solution with the W atom concentrations of 0.50, 0.05 and 0.005 mol L^{-1} for 5 h, respectively (W atom concentration equals 1/7 AMT concentration, for one AMT molecule having seven W atoms). The exchanged resin was washed with deionized water and dried at 80 °C overnight. The dried resin was then heated at 600 °C for 1 h in N_2 atmosphere. After cooling down to room temperature, the resulting product was grinded into powders and the final tungsten oxide on carbonized resin composite (C-WO_3) was obtained. The C-WO_3 prepared with the W atom concentrations of 0.50, 0.05 and 0.005 mol L^{-1} were denoted as C-WO_3(0.50), C-WO_3(0.05) and C-WO_3(0.005), accordingly.

Pt supported on C-WO_3 (denoted as Pt/C-WO_3) was prepared and used as electrocatalyst for ORR. A total of 50 mg of C-WO_3 was added in a mixed solution with H_2PtCl_4 (58 mg) and formic acid and treated in ultrasonic bath for 30 min to form uniform ink. After the ink was dried, we got Pt/C-WO_3 electrocatalyst. The Pt contents in the resulting products were targeted at 40 wt%. The actual Pt contents were determined by inductively coupled plasma-atomic emission spectrometry (ICP, IRIS (HR), USA).

For electrode preparation, Pt/C-WO_3 (5 mg) or commercial Pt/C (4 mg, 47.6 wt % Pt, TKK, Japan) were dispersed in 1.95 ml of ethanol and 0.05 ml of 5 wt% Nafion suspension (DuPont, USA) under ultrasonic agitation to form the electrocatalyst ink. The electrocatalyst ink (5 μl) was deposited on the surface of a rotating disk electrode and dried at room temperature. The total Pt loadings were controlled at 0.02 mg cm^{-2}.

The electrochemical measurements were carried out in an oxygen-saturated 0.1 mol L^{-1} $HClO_4$ solution scanned between 0 and 1.1 V (vs. RHE) at a scan rate of 5 mV s^{-1} at 25 °C controlled by a water-bath thermostat. A platinum foil (1.0 cm^2) and a reversible hydrogen electrode (RHE) were used as counter and reference electrodes, respectively.

All chemicals were of analytical grade and used as received.

The morphologies and sizes of the C-WO_3 and Pt supported electrocatalysts were characterized by transmission electron microscopy (TEM, JOEP JEM-2010, JEOL Ltd.) operating at 200 kV. The structure of C-WO_3 and electrocatalysts were determined on a X-ray diffractometer (XRD, D/Max-IIIA, RigakuCo., Japan,CuK1, $\lambda = 1.54056$ Å radiation) and a X-ray Photoelectron Spectroscopy (XPS, ESCALAB 250, Thermo-VG Scientific).

3. Results and discussion

Fig. 1a and b show the XRD patterns of C-WO_3(0.50), C-WO_3(0.05) and C-WO_3(0.005). All the patterns match the characteristics of WO_3 crystal (PDF#20-1324) by comparing JCPDS cards. The peak intensities of the WO_3 weakened with the decreasing concentration of AMT, which related to the particle size.

Fig. 2 shows the TEM images of the WO_3 nanoparticles on carbonized resin, which were prepared at different concentrations of AMT. As shown in Fig. 2a, the C-WO_3(0.50) prepared at higher concentration of AMT carried large and congregated bulks of WO_3 crystals. The morphology of the WO_3 crystals could transform to less sized nanobars with the length of 10–50 nm and width of 3–6 nm with the reduction in AMT concentrations (Fig. 2b). And the less concentration is AMT, the more sparse distribution is WO_3 nanoparticles (Fig. 2c). Fig. 2d shows the HRTEM image of C-WO_3(0.05), the crystal lattice of WO_3 (200) is clearly shown.

The reason for the different shape of WO_3 particles at different AMT concentrations is tried to explain as follows. The D201 × 1 cinnamic strong alkali anion exchange resin has long-chain structure (see Fig. 3), which would combine the $W_7O_{24}^{6-}$ ions linearly through ion exchanging. After the exchanged resin is carbonized, the bar-shaped WO_3 particles will accordingly form. But if the concentration of AMT is too low, the formed WO_3 particles could not link each other to form bars. So there are lots of dot-shaped

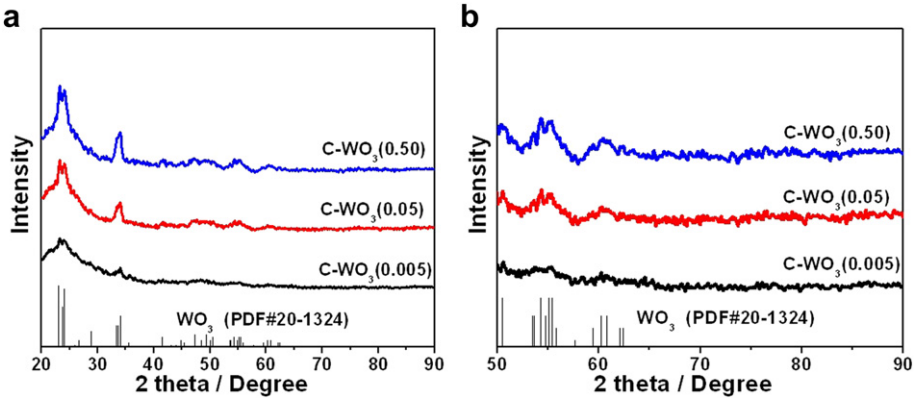

Fig. 1. (a) XRD patterns of C-WO_3 composite with different AMT concentrations and (b) the corresponding XRD patterns at high angle range.

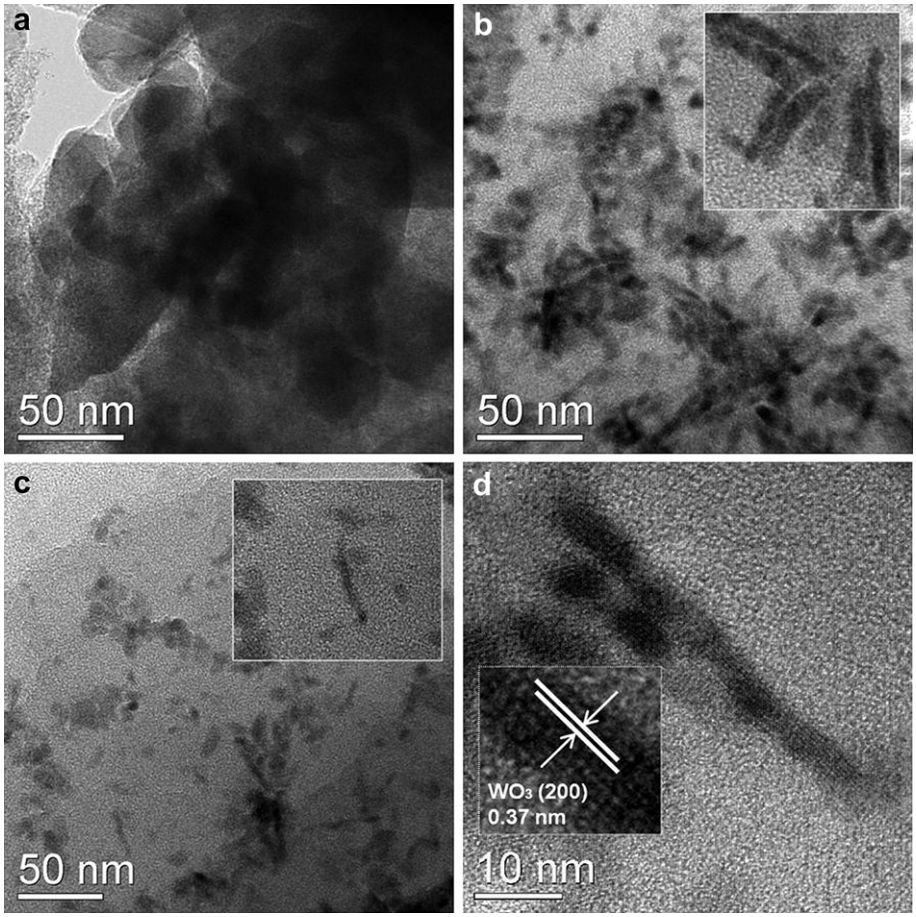

Fig. 2. TEM images of (a) C-WO_3(0.50), (b) C-WO_3(0.05) and (c) C-WO_3(0.005), (d) HRTEM image of C-WO_3(0.50). Insets are the magnified images correspondingly.

WO_3 particles in C-WO_3(0.005) (Fig. 2c). However, when the AMT concentration is too high, the WO_3 bars would congregate to bulks (Fig. 2a).

The original C-WO_3(0.50), C-WO_3(0.05) and C-WO_3(0.005) composites were used as alternative supporting materials replacing amorphous carbon to load Pt nanoparticles for electrocatalysis. Fig. 4 shows the TEM images of Pt loaded C-WO_3 including Pt/C-WO_3(0.50), Pt/C-WO_3(0.05) and Pt/C-WO_3(0.005). It can be seen that the Pt nanoparticles with the diameter about 3 nm were uniformly dispersed on the C-WO_3 matrix, which could exert the promotion effect between WO_3 and Pt on electrochemical catalytic performance. When the C-WO_3 was prepared with high concentration of AMT, it is not easy to identify the Pt and WO_3 particles in the TEM image (Fig. 4a). The WO_3 particles in C-WO_3(0.50) are much larger in size which result in higher density of the matrix (Fig. 2a) and worsen the dispersion of Pt nanoparticles (Fig. 4a), and would consequently reduce the promotion effect on Pt. However, when the C-WO_3 was prepared with low concentrations of AMT such as C-WO_3(0.05) and C-WO_3(0.005), the WO_3 particles are smaller in size (Fig. 2b, c), resulting in better dispersion of Pt nanoparticles (Fig. 4b, c). The inset EDS pattern of Pt/C-WO_3(0.05) in Fig. 4b confirms the coexistence of Pt, C, W and O elements. In addition, the peaks of Cu and Cr elements come from sample bracket. Fig. 4d shows the HRTEM image of Pt/C-WO_3(0.05), the crystal lattice of WO_3 (001) and Pt (111) are clearly shown, which further confirm the existence of WO_3 and Pt. Fig. 4b and d also show three different supporting locations of Pt particles. A great number of Pt particles are supported on carbon, which are similar as the common Pt/C catalyst; few on WO_3, which might have no activity for the very low electric conductivity of WO_3 ($\sim 6 \times 10^{-8}$ S cm^{-1}); and some on the adjacent area of carbon and WO_3, which could have both well electric conductivity and synergistic effect. Because WO_3 nanobars are very thin (3–6 nm), most of the Pt particles (3–4 nm) on WO_3 nanobars could touch the carbon around and therefore could have well electric conductivity and synergistic effect.

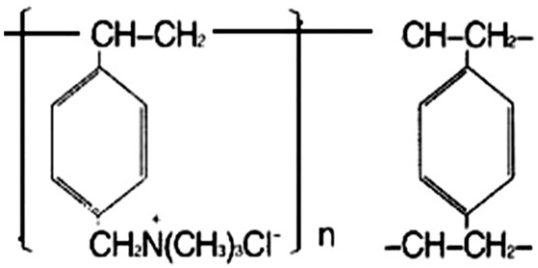

Fig. 3. The structural formula of D201 × 1 cinnamic strong alkali anion exchange resin.

Fig. 5a and b show the XRD patterns of the Pt/C-WO_3(0.50), Pt/C-WO_3(0.05) and Pt/C-WO_3(0.005). The peaks of WO_3 and Pt are partially overlapped. The dominating Pt 2θ peak is at 39.8°, which corresponds to (111) crystal lattice of Pt. The 2θ peaks at 46.2°, 67.5°, 81.2° and 85.7° which correspond to (200), (220), (311) and (222) facets of Pt, are hardly discerned. This result suggests that Pt

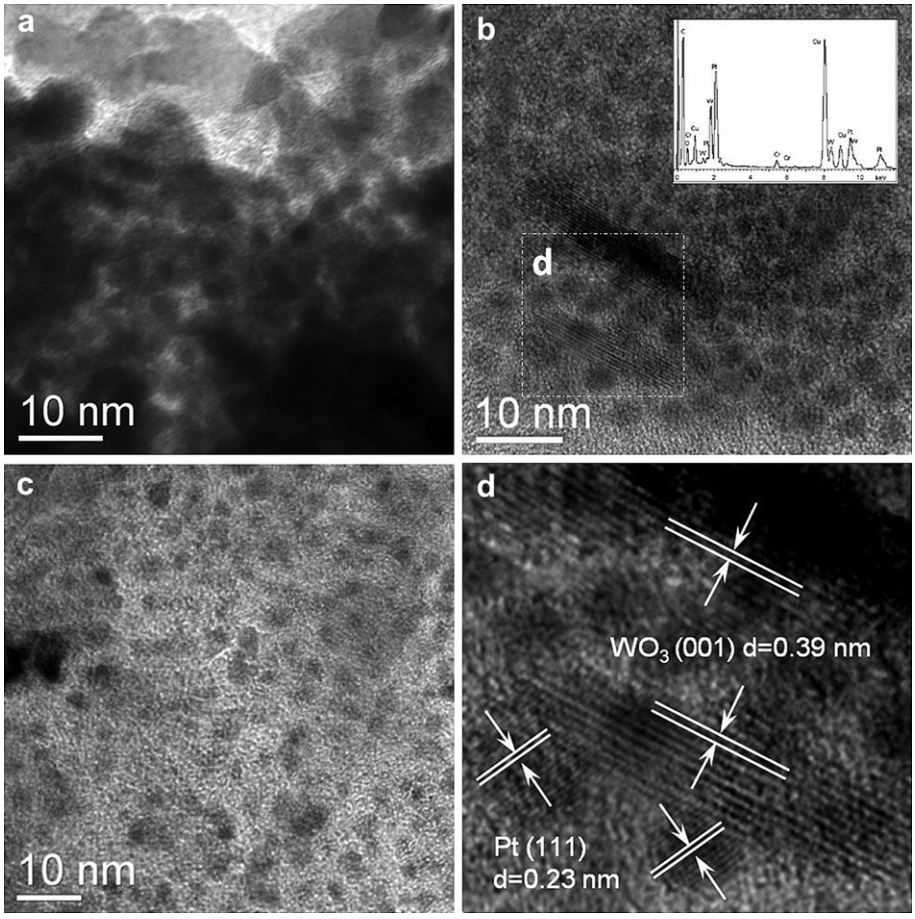

Fig. 4. TEM images of (a) Pt/C-WO_3(0.50), (b) Pt/C-WO_3(0.05) (inset is the corresponding EDS pattern) and (c) Pt/C-WO_3(0.005), and (d) HRTEM image of Pt/C-WO_3(0.05).

nanoparticles deposited on C-WO_3 are dominated with Pt (111) plane, which has been approved to be the most active lattice site for oxygen reduction reaction [48].

Fig. 6 shows the XPS spectras of the Pt 4f on Pt/C and Pt/C-WO_3(0.05). The peaks on Pt/C at 71.0 eV and 74.3 eV belong to metallic Pt, and the peaks at 72.5 eV and 75.7 eV belong to Pt(II) [49]. However, the Pt/C-WO_3 has the peaks at 71.3 eV and 74.6 eV for metallic Pt, and 72.8 eV and 76.0 eV for Pt(II). Obviously, positive shift occurred in XPS spectra after the introduction of WO_3. The result indicates that there is an increased interaction between Pt and WO_3 comparing that between Pt and C, which might result in an increased electrochemical activity and stability for Pt/C-WO_3.

The electrocatalyst performance on ORR could be improved by the introduction of catalyst promoter [50–53]. The Pt/C-WO_3 samples prepared by present method were further tested as electrocatalysts for ORR. Fig. 7a shows the linear polarization curves of ORR on Pt/C-WO_3(0.50), Pt/C-WO_3(0.05), Pt/C-WO_3(0.005) and commercial Pt/C electrodes in O_2 saturated 0.1 mol L^{-1} $HClO_4$ solution with a scan rate of 5 mV s^{-1} from 0 to 1.1 V (vs. RHE) and rotating speed of 1600 rpm min^{-1} at 25 °C. Fig. 7b shows the kinetic

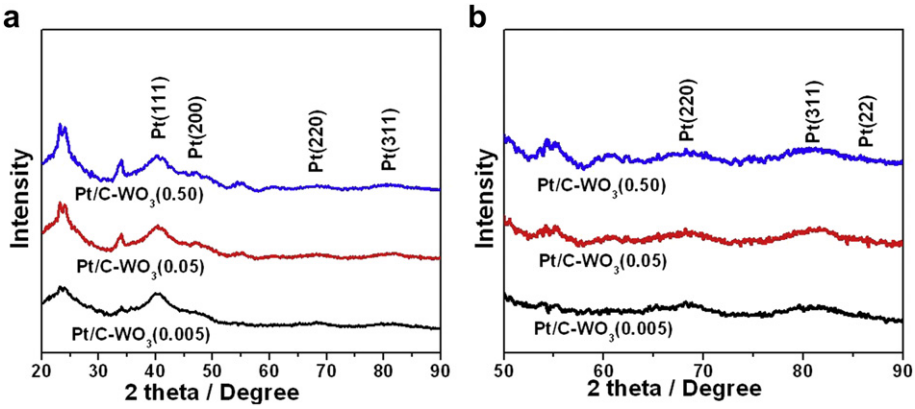

Fig. 5. (a) XRD pattern of Pt/C-WO_3 electrocatalysts with different AMT concentrations and (b) the corresponding XRD patterns at high angle range.

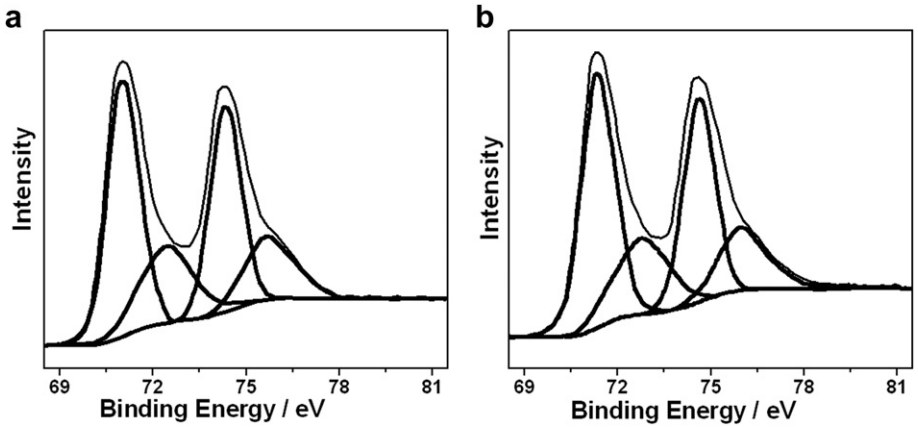

Fig. 6. XPS spectras of the Pt 4*f* on (a) Pt/C and (b) Pt/C-WO_3(0.05)

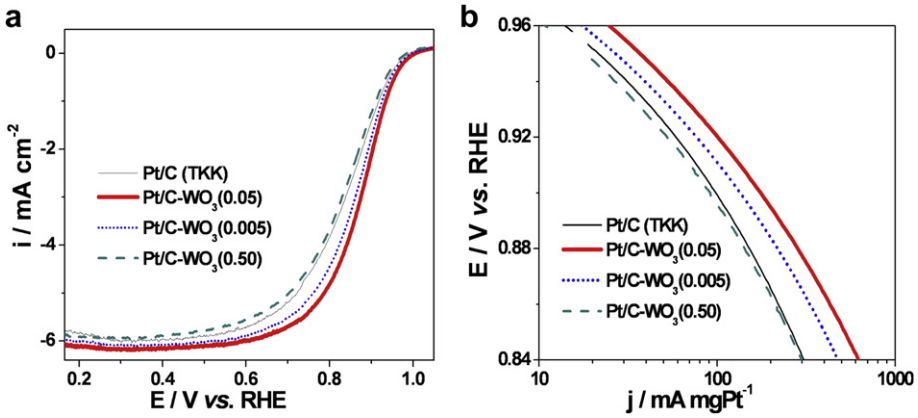

Fig. 7. (a) The ORR on Pt/C-WO_3(0.50), Pt/C-WO_3(0.05), Pt/C-WO_3(0.005) and Pt/C electrodes in O_2 saturated 0.1 mol L^{-1} $HClO_4$ solution, 25 °C, scan rate: 5 mV s^{-1}, 1600 rpm min^{-1}, (b) the corresponding mass activity–potential plots.

currents of the electrocatalysts calculated from the experimental data using the well-known mass-transport correction for rotating disk electrode [54]:

$$i_k = i_d i/(i_d - i) \quad (1)$$

where i is the experimentally obtained current, i_d refers to the measured diffusion-limited current and i_k the mass-transport-free kinetic current. The mass activity (i_m) can be determined via the calculation of i_k using Eq. (1) and normalized to the Pt loadings. The kinetic currents measured from the curves in Fig. 7b are summarized in Table 1. Among the three Pt/C-WO_3 electrocatalysts, Pt/C-WO_3(0.05) has the highest catalytic activity for ORR and the Pt-mass activity is measured as 174.6 mA mg^{-1}_{Pt}. The Pt/C-WO_3(0.005) is not as good as Pt/C-WO_3(0.05) for ORR, because too less WO_3 to promote the synergistic effect on Pt. Similarly, the worse performance of Pt/C-WO_3(0.50) is due to the larger WO_3 particles which are not efficient in promoting the synergistic effect. In this study, the measured activity of the commercial Pt/C electrocatalyst is fairly close to the published value in literatures [48,55].

Table 1
The performance comparison of the four electrocatalysts.

Electrocatalyst	Pt-mass content[a]	i_m at 0.9 V (mA mg^{-1}_{Pt})
Pt/C-WO_3(0.50)	34.6%	91.7
Pt/C-WO_3(0.05)	37.0%	174.6
Pt/C-WO_3(0.005)	36.8%	134.6
Pt/C-TKK	47.6%	98.6

[a] The data were determined by inductively coupled plasma-atomic emission spectrometry (ICP).

The stabilities of the Pt/C-WO_3(0.05) and Pt/C electrodes for ORR with the potential scan range from 0 to 1.1 V (vs. RHE) by comparing the 1st and the 3000th cyclic voltammogram cycles are shown in Fig. 8a. The kinetic currents measured from the curves in Fig. 8b are summarized in Table 2. It can be seen that both Pt/C-WO_3(0.05) and Pt/C decreased in activity after being performed for 3000 cycles. It is clear that the activity of the commercial Pt/C reduced 9.6% from 98.6 mA mg^{-1}_{Pt} to 89.1 mA mg^{-1}_{Pt} by comparing the Pt-mass activity at 0.9 V. However, the activity of the Pt/C-WO_3(0.05) reduced 7.1% from 174.6 mA mg^{-1}_{Pt} to 162.2 mA mg^{-1}_{Pt}. The results indicate that the Pt/C-WO_3 electrocatalyst is more stable than the commercial Pt/C electrocatalyst, despite the possible relative errors.

The promotion effect of WO_3 on Pt electrocatalyst in activity and durability is consistent with the reported literatures [37–39]. On one hand, WO_3 plays the role of donor of the oxygen-containing species and increases the oxygen concentration which reduces the reaction activity energy and improves the limiting current densities [56,57]. On the other hand, there is a stronger interaction between Pt and WO_3 than that between Pt and C (Fig. 6), and consequently promotes the electrochemical stability.

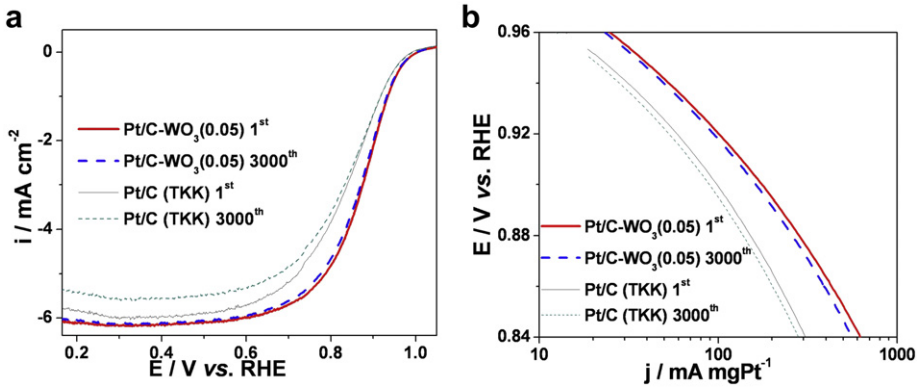

Fig. 8. The ORR on Pt/C-WO_3(0.05) and Pt/C electrodes at 1st and 3000th cyclic voltammogram cycles in O_2 saturated 0.1 mol L^{-1} $HClO_4$ solution with the scan rate of 5 mV s^{-1} at 25 °C, 1600 rpm min^{-1}.

Table 2
The electrochemical stability comparison of Pt/C-WO3(0.05) and Pt/C electrocatalysts.

Electrocatalyst	CV cycle	i_m at 0.9 V (mA mg_{Pt}^{-1})	Reduced activity
Pt/C-WO_3(0.05)	1st	174.6	7.1%
Pt/C-WO_3(0.05)	3000th	162.2	
Pt/C	1st	98.6	9.6%
Pt/C	3000th	89.1	

4. Conclusions

Tungsten oxide nanobars with the length of 10–50 nm and the width of 3–6 nm supported on carbonized resin (C-WO_3) were synthesized through an ionic exchange route to locally anchor the metatungstate ions. The produced WO_3 crystals could have dot, bar or bulk shapes, which can be easily controlled by adjusting the concentration of the metatungstate ions. Pt nanoparticles were supported on the C-WO_3 composites (Pt/C-WO_3) and used as electrocatalyst for ORR. The results showed that WO_3 with moderate concentration could give the best promotion effect on Pt supported electrocatalyst. A typical Pt/C-WO_3(0.05) electrocatalyst gives the kinetic mass current of 174.6 mA mg^{-1}_{Pt}, which is much higher than that of commercial Pt/C electrocatalyst (98.6 mA mg^{-1}_{Pt}) for ORR at the same Pt loadings. Moreover, the electrochemical stability of Pt/C-WO_3 is more excellent than that of Pt/C. The higher catalytic activity and chemical stability may be due to the promotion effect of WO_3 nanobars on Pt and the strong interaction force between WO_3 and Pt respectively. The present method is simple and effective, which can be readily scale up for the production of other nanomaterials as well as WO_3.

Acknowledgements

This work was financially supported by Research Foundation for Talented Scholars of Jiangsu University (11JDG142), Science and Technology Support Program of Jiangsu (BE2010144), Natural Science Foundation of Jiangsu (BK2010166) and Doctoral Fund from National Ministry of Education (20093227110009), China. Dr. X.M. Lü is gratefully acknowledge the financial support by National Natural Science Foundation of China (no. 21003065).

References

[1] Z. Yan, C. Wang, P.K. Shen, International Journal of Hydrogen Energy 37 (2012) 4728–4736.
[2] H. Meng, C.X. Wang, P.K. Shen, G. Wu, Energy and Environmental Science 4 (2011) 1522–1526.
[3] X. Ma, H. Meng, M. Cai, P.K. Shen, Journal of American Chemical Society 134 (2012) 1954–1957.
[4] Y. Yu, H. Li, H. Wang, X.Z. Yuan, G. Wang, M. Pan, Journal of Power Sources 205 (2012) 10–23.
[5] A.M. Bartrom, J.L. Haan, Journal of Power Sources 214 (2012) 68–74.
[6] Z. Yan, Z. Hu, C. Chen, H. Meng, P.K. Shen, H. Ji, Y. Meng, Journal of Power Sources 195 (2010) 7146–7151.
[7] G. He, Z. Yan, X. Ma, H. Meng, P.K. Shen, C. Wang, Nanoscale 3 (2011) 3578–3582.
[8] Y. Huang, H. Huang, Y. Liu, Y. Xie, Z. Liang, C. Liu, Journal of Power Sources 201 (2012) 81–87.
[9] J. Zhao, K. Jarvis, P. Ferreira, A. Manthiram, Journal of Power Sources 196 (2011) 4515–4523.
[10] S.B. Yin, M. Cai, C.X. Wang, P.K. Shen, Energy and Environmental Science. 4 (2011) 558–563.
[11] M. Oezaslan, P. Strasser, Journal of Power Sources 196 (2011) 5240–5249.
[12] F.J. Perez-Alonso, C.F. Elkjær, S.S. Shim, B.L. Abrams, I.E.L. Stephens, I. Chorkendorff, Journal of Power Sources 196 (2011) 6085–6091.
[13] J.L. Qiao, R. Lin, B. Li, J.X. Ma, J.S. Liu, Electrochimica Acta 28 (2010) 8490–8497.
[14] J. Snyder, T. Fujita, M.W. Chen, J. Erlebacher, Nature Materials 9 (2010) 904–907.
[15] V. Mazumder, M. Chi, K.L. More, S. Sun, Angewandte Chemie International Edition 49 (2010) 9368–9372.
[16] X. Li, Z. Lin, L. Yi, J. Lu, H.D. Abruna, Journal of American Chemical Society 131 (2009) 602–608.
[17] Y. Liu, S. Shrestha, W.E. Mustain, ACS Catalysis 10 (2012) 456–463.
[18] Z. Yan, M. Cai, P.K. Shen, Journal of Materials Chemistry 22 (2012) 2133–2139.
[19] I.S. Song, S.W. Heo, J.R. Ku, D.K. Moon, Thin Solid Films 520 (2012) 4068–4073.
[20] Y.D. Ko, K.C. Kim, Y.S. Kim, Superlattices and Microstructures 51 (2012) 933–941.
[21] R. Scott, S.D. Cherico, Iron and Steel Technology 4 (2007) 315–324.
[22] X. Lü, J. Liu, J. Zhu, D. Jiang, J. Xie, Journal of Materials Research 25 (2010) 104–109.
[23] M. Risch, D. Shevchenko, M.F. Anderlund, S. Styring, J. Heidkamp, K.M. Lange, A. Thapper, I. Zaharieva, International Journal of Hydrogen Energy 37 (2012) 8878–8888.
[24] J. Xie, D. Jiang, M. Chen, D. Li, J. Zhu, X. Lü, C. Yan, Colloids and Surfaces A 372 (2010) 107–114.
[25] C. Feng, Y. Zhang, S. Liu, Z. Chi, J. Xu, Polymer Degradation and Stability 97 (2012) 707–714.
[26] W.D. Huang, H. Cao, S. Deb, M. Chiao, J.C. Chiao, Sensors and Actuators, A: Physical 169 (2011) 1–11.
[27] K. Wetchakun, T. Samerjai, N. Tamaekong, C. Liewhiran, C. Siriwong, V. Kruefu, A. Wisitsoraat, A. Tuantranont, S. Phanichphant, Sensors and Actuators, B: Chemical 160 (2011) 580–591.
[28] T. Stoycheva, S. Vallejos, C. Blackman, S.J.A. Moniz, J. Calderer, X. Correig, Sensors and Actuators, B: Chemical 161 (2012) 406–413.
[29] J. Chen, H. Ye, L. Aé, Y. Tang, D. Kieven, T. Rissom, J. Neuendorf, M.C. Lux-Steiner, Solar Energy Materials and Solar Cells 95 (2011) 1437–1440.
[30] Y. Liu, H. Liu, J. Ma, J. Li, Journal of Hazardous Materials 213, 214 (2012) 222–229.
[31] X. Du, X. Gao, L. Cui, Y. Fu, Z. Luo, K. Cen, Fuel 92 (2012) 49–55.
[32] C. Pan, Y. Li, Y. Ma, X. Zhao, Q. Zhang, Journal of Power Sources 196 (2011) 6228–6231.
[33] E.J. McLeod, V.I. Birss, Electrochimica Acta 51 (2005) 684–693.
[34] W.J. Long, M.R. Stroud, E.K. Swider-Lyons, R.D. Rolison, Journal of Physical Chemistry B 104 (2000) 9772–9776.
[35] P.K. Shen, A.C.C. Tseung, Journal of Electrochemical Society 141 (1994) 3082–3090.

[36] M. Gotz, H. Wendt, Electrochimica Acta 43 (1998) 3637–3644.
[37] S. Jayaraman, T.F. Jaramillo, S.H. Baeck, E.W. McFarland, Journal of Physical Chemistry B 109 (2005) 22,958–22,966.
[38] F. Maillard, E. Peyrelade, Y. Soldo-Olivier, M. Chatenet, E. Chainet, R. Faure, Electrochimica Acta 52 (2006) 1958–1967.
[39] M.S. Saha, Y. Zhang, M. Cai, X. Sun, International Journal of Hydrogen Energy 37 (2012) 4633–4638.
[40] M.S. Saha, M.N. Banis, Y. Zhang, R. Li, X. Sun, M. Cai, F.T. Wagner, Journal of Power Sources 192 (2009) 330–335.
[41] H. Zheng, J.Z. Ou, M.S. Strano, R.B. Kaner, A. Mitchell, K. Kalantar-zadeh, Advanced Functional Materials 21 (2011) 2175–2196.
[42] O. Savadogo, P. Beck, Journal of Electrochemical Society 143 (1996) 3842–3846.
[43] Chao Zhang, Abdelhamid Boudiba, Cristina Navio, Carla Bittencourt, Marie-Georges Olivier, Rony Snyders, Marc Debliquy, International Journal of Hydrogen Energy 36 (2011) 1107–1114.
[44] A.E. Kadib, A. Primo, K. Molvinger, M. Bousmina, D. Brunel, Chemistry – A European Journal 17 (2011) 7940–7946.
[45] C. Sui, J. Gong, T. Cheng, G. Zhou, S. Dong, Applied Surface Sciences 257 (2011) 8600–8604.
[46] Z. Yan, H. Meng, P.K. Shen, R. Wang, L. Wang, K. Shi, H. Fu, Journal of Materials Chemistry 22 (2012) 5072–5079.
[47] Z. Yan, M. Cai, P.K. Shen, Journal of Materials Chemistry 21 (2011) 19,166–19,170.
[48] H.A. Gasteiger, S.S. Kocha, B. Sompalli, F.T. Wagner, Applied Catalysis B 56 (2005) 9–35.
[49] L. Ma, X. Zhao, F. Si, C. Liu, J. Liao, L. Liang, W. Xing, Electrochimica Acta 55 (2010) 9105–9112.
[50] K. Gong, F. Du, Z. Xia, M. Durstock, L. Dai, Science 323 (2009) 760–764.
[51] J. Zhang, K. Sasaki, E. Sutter, R.R. Adzic, Science 315 (2007) 220–222.
[52] M. Lefèvre, E. Proietti, F. Jaouen, J.P. Dodelet, Science 324 (2009) 71–74.
[53] D. Strmcnik, M. Escudero-Escribano, K. Kodama, V.R. Stamenkovic, A. Cuesta, N.M. Markovic, Nature Chemistry 2 (2010) 880–885.
[54] S. Chouzier, P. Afanasiev, M. Vrinat, T. Cseri, M. Roy-Auberger, Journal of Solid State Chemistry 179 (2006) 3314–3323.
[55] B. Lim, M.J. Jiang, P.H.C. Camargo, E.C. Cho, J. Tao, X.M. Lu, Y.M. Zhu, Y.A. Xia, Science 324 (2009) 1302–1305.
[56] D.S. Kim, E.F.A. Zeid, Y.T. Kim, Electrochimica Acta 55 (2010) 3628–3633.
[57] M. Montiel, P. Hernández-Fernández, J.L.G. Fierro, S. Rojas, P. Ocón, Journal of Power Sources 191 (2009) 280–288.